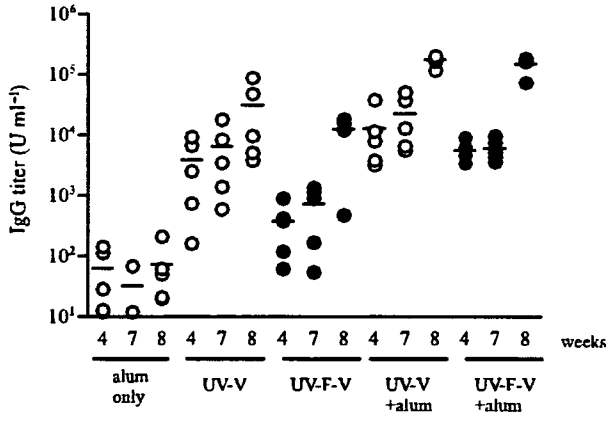

Fig. 1. Effect of formalin treatment of the UV-V vaccine on the SARS-specific IgG response by subcutaneously immunized mice. Mice (five mice in each group) were primed subcutaneously with 10 μg of the UV-V or UV-F-V preparations with or without 2 mg of alum, or injected with alum alone, and then boosted in their footpads with the same preparation 7 weeks after priming. Their sera were collected 4, 7, and 8 weeks after the primary immunization and subjected to ELISA to detect SARS-specific IgG. The ELISA employed SARS-CoV-infected Vero E6 cell lysates as the coating antigen. The circles and bars represent the IgG antibody levels in the serum of each mouse and the mean levels, respectively. The IgG levels were calculated on the basis of a hyperimmune serum standard. Representative results of two independent experiments are shown. ns, statistically not significant ($P > 0.05$), as determined by unpaired t test.

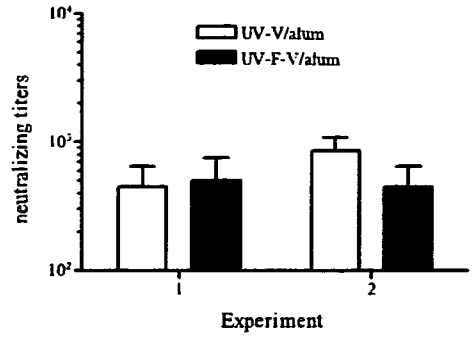

Fig. 2. The neutralizing activity induced by formalin treated UV-V vaccine was similar to that induced by UV-V vaccine. Serum samples of five mice immunized twice either with UV-V+alum or UV-F-V+alum at 1 week after booster vaccination were incubated with SARS-CoV for 1 h at 37°C, and then added to the Vero E6 cell culture. The titer is a reciprocal number of minimum serum dilution that inhibits the cytopathic effect. The results of two independent experiments were shown. Standard deviation was depicted by bars. The difference between UV-V- (open column) and UV-F-V- (closed column) immunized group was not statistically significant ($P > 0.05$).

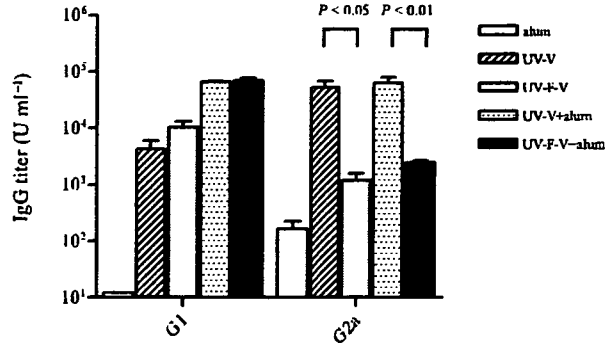

Fig. 3. SARS-CoV-specific IgG_{2a} antibodies are induced by UV-V but not by UV-F-V. Sera collected from mice immunized as described in the legend to Figure 1 were subjected to ELISA to detect the SARS-CoV-specific IgG_1 and IgG_{2a} titers. The units in each ELISA were determined as described above. The columns and bars indicate the mean serum titers in each group and the standard deviation, respectively. The results shown are representative of two separate experiments.

serum (Fig. 1). The alum adjuvant enhanced the IgG antibody levels induced by both vaccines. These findings confirmed our previous observations made with the UV-V vaccine (14). Just prior to boosting the mice at week 7, all vaccinated groups of mice (with the exception of the alum-only control group) showed modest elevations in anti-SARS CoV IgG antibody levels, and 1 week after the boost, the anti-SARS CoV IgG antibody levels in all UV-F-V and UV-V vaccinated mice were markedly elevated (i.e., at least 10-fold above the primary response) (Fig. 1). The difference between UV-F-V-immunized and UV-V-immunized mice in terms of their IgG responses was statistically non-significant ($P > 0.05$) at all time points (with or without alum), and high levels of serum antibody were maintained for more than 6 months. Moreover, analysis of the neutralizing capacity of the 8 week sera samples from the UV-V and UV-F-V vaccinated mice revealed similar neutralizing activities (Fig. 2). Thus, it appears that formalin treatment of the whole killed SARS-CoV vaccine to ensure virus killing has little effect on the humoral immunogenicity of the vaccine.

Formalin treatment of the UV-inactivated SARS-CoV vaccine induces a weak IgG_{2a} subclass antibody response, unlike the UV-V vaccine: We then measured the SARS CoV-specific IgG_1, G_{2a}, G_{2b}, G_3, and A immunoglobulin subclasses in the serum of the five groups of mice 1 week after they had received the booster vaccination. The mice inoculated with UV-V and UV-F-V had similar levels of SARS CoV-specific IgG_1 antibody, and alum further increased these levels (Fig. 3). In contrast, the UV-F-V-immunized mice had 40-fold lower levels of anti-SARS-CoV IgG_{2a} than the UV-V-immunized mice (Fig. 3). Moreover, the presence of alum did not change the anti-SARS-CoV IgG_{2a} levels in the UV-V- and UV-F-V-immunized mice (Fig. 3). This findinf is consistent with what we observed previously with regard to the UV-V vaccine (14). The anti-SARS-CoV IgG_{2b}, IgG_3, and IgA antibody levels were low or undetectable in both groups. Thus, our results suggest that the balanced (Th0) type immune response that is elicited by UV-V+alum tends to skew towards a Th2-type response with formalin treatment of the vaccine preparation.

Mice immunized with UV-F-V have similar frequencies of antibody-producing cells in the bone marrow as do those immunized with UV-V: The N protein is one of the major antigenic determinants of SARS-CoV, and SARS patients frequently have serum antibodies against this protein (16,17). This suggests that anti-N antibodies may be useful as a sensitive diagnostic marker of SARS-CoV infection, even though these antibodies do not appear to play a significant role in protection from disease (11,13,18-20). In order to map the immunodominant humoral epitopes on the N protein, we prepared four recombinant N proteins: one was the full-length protein, and the other three were truncated from the N- or C-termini, and were designated as N1, N2, and N3. All were fused with a 6xHistidine tag and SUMO protein (total 13 kDa) at their N-termini (Fig. 4A). When we measured the anti-N serum antibodies in UV-V- and UV-F-V-vaccinated mice using a mixture of N2 and N3, the results paralleled the measurements obtained by using SARS-CoV-infected Vero E6 cell lysates as described above (data not shown). Western

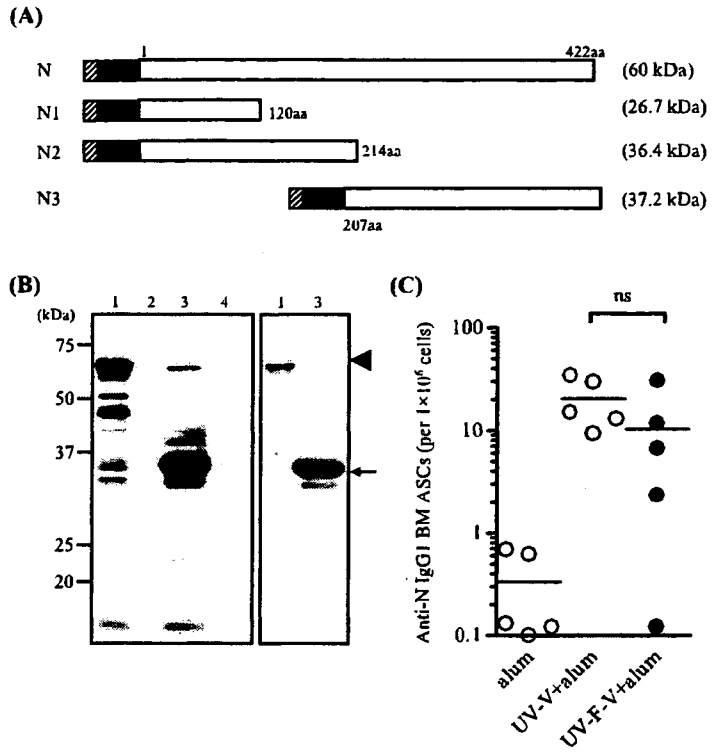

Fig. 4. UV-F-V- and UV-V-vaccinated mice have similar numbers of SARS-CoV-specific IgG_1 plasma cells in their bone marrow, as detected by an ELISPOT assay employing recombinant N2 protein. (A) The predicted structure of recombinant N proteins obtained from bacteria by using the pET-SOMO System (Invitrogen). The N-termini of the recombinant proteins are fused with a His tag (shadowed) and the SUMO protein (black). The total size of each protein is indicated in parentheses. (B) Western blot analysis to identify the epitope recognized by the anti-N mAb SKOT-9. The bacterial lysates expressing recombinant N proteins (left panel) or purified N and N2 proteins (right panel) were separated by SDS-PAGE and blotted onto PVDF membranes. The membranes were then incubated with the anti-N mAb SKOT-9, followed by incubation with HRP-conjugated anti-mouse IgG antibody. The signal was visualized by a Super Signal Western Dura Extended Duration Substrate (Pierce) by using an LAS3000 analyzer (Fuji Film). Lane 1, N (arrow head); lane 2, N1; lane 3, N2 (arrow); and lane 4, N3. (C) Mice were primed and boosted by subcutaneous injection on their back with 10 μg of UV-V or UV-F-V with 2 mg of alum (VA). The bone marrow cells were collected 7 days after the booster shot and subjected to ELISPOT to detect the SARS-CoV-specific IgG_1 plasma cells. Each circle represents an individual mouse and the bars indicate the mean spot-forming cell numbers in each group. Representative results of two independent experiments are shown. ASC, antibody secreting cell.

blot analysis of the recombinant N proteins using anti-N mAb, SKOT-8 or SKOT-9 (15), revealed that both mAbs reacted exclusively with N2, but not with N1 (Fig. 4B and data not shown). Thus, a major antibody determinant of the N protein in BALB/c mice is located in the N-terminal half of the protein near its center.

Our previous study showed that the bone marrow of mice immunized with UV-V+alum contains a small number of cells that produce antibodies specific for a 49-mer N peptide (14). To investigate whether UV-F-V, like UV-V, can generate long-term antibody-producing cells, we subjected samples from UV-F-V+alum- and UV-V+alum-immunized mice to an ELISPOT assay that detects SARS-CoV-specific plasma cells in mouse bone marrow. In a preliminary experiment using mice immunized twice with UV-V+alum, we found that the SARS-CoV-specific antibody-producing cells in the bone marrow were most efficiently detected when the ELISPOT plate membrane was coated with N2; in contrast, N1, N3, and the 1-49 amino acid N peptide were found to be less effective as coating antigens. Thus, bone marrow cells were obtained from the UV-F-V+alum- and UV-V+alum-immunized mice after the booster immunization, and the frequency of N2-specific antibody-producing cells was then analyzed. The two groups of mice exhibited similar frequencies of SARS-CoV-specific IgG_1 plasma cells in the bone marrow (Fig. 4C). This mimicks the anti-SARS-CoV IgG responses in the serum (Fig. 1). Taken together, these observations suggest that the UV-V and UV-F-V vaccine are equivalent with respect to their ability to elicit potentially long-lived SARS-CoV-specific antibody-producing cells in the bone marrow, as suggested by others in the LCMV infection (21).

Formalin treatment of the UV-inactivated vaccine skews the T-cell cytokine response towards the Th2 type: We also analyzed the T-cell cytokine responses in UV-F-V+alum- and UV-V+alum-vaccinated mice. Seven days after receiving the second subcutaneous booster, the mice were sacrificed and their T cells from pooled regional lymph nodes (axillar or cervical) were enriched (>95%) and cultured with irradiated splenic non-T cell APCs in the presence or absence of UV-V at 10 μg ml^{-1}. The culture supernatants were collected on day 4, and the IFN-γ, TNF-α, IL-2, IL-4, and IL-5 levels in the supernatants were measured by a CBA kit. The T cells from the cervical lymph nodes produced only small amounts of all five cytokines (data not shown). Representative results of two experiments examining the axillar T-cell cytokine responses are shown in Figure 5. The axillar T cells of both vaccinated groups constitutively produced high levels of IL-2, and re-stimulation with virion in vitro negligibly elevated these responses. With regard to IFN-γ, neither vaccine generated high levels (under 200 pg ml^{-1}); this result stood in contrast to the ng levels of IFN-γ produced upon vaccination with live or inactivated influenza virus (22). Moreover,

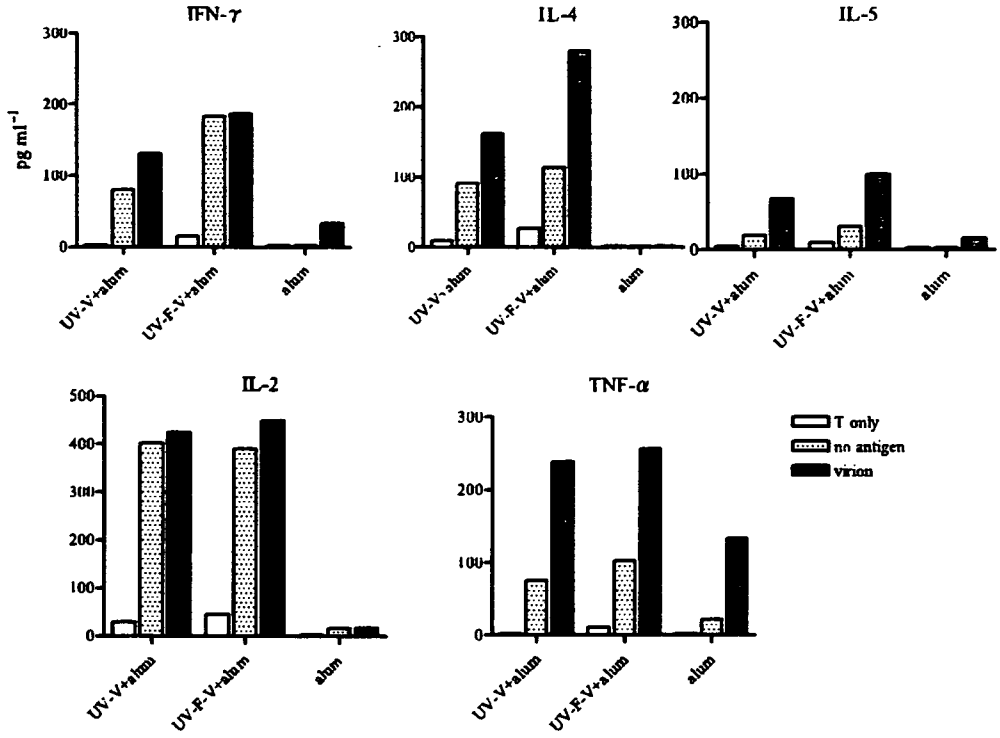

Fig. 5. UV-F-V induces more IL-4 production than the UV-V vaccine. Mice were subcutaneously primed with 10 μg of UV-V or UV-F-V with alum, or with alum only, and then boosted with the same antigen on their back 7 weeks after priming. The axillar lymph nodes isolated 1 week after the boost were pooled and T cells were enriched (>95% purity). These T cells were stimulated for 4 days with T-cell-depleted syngeneic splenocytes that had been pulsed with 10 μg ml^{-1} of UV-V. The levels of IFN-γ, IL-2, IL-4, IL-5, and TNF-α in the culture supernatants were determined by using a CBA kit. The results shown are representative of two separate experiments. "T only" indicates purified T cells cultured in the absence of APCs and virion.

re-stimulation with virion in vitro only slightly affected the IFN-γ responses. In contrast, the axillar T cells of the UV-F-V+alum-vaccinated mice produced more IL-4 in an antigen-dependent manner than did the axillar T cells of the UV-V+alum-immunized mice. However, neither group produced much IL-5. As regards TNF-α production, both groups showed similar levels. Moreover, even the alum-only-immunized mice produced substantial amounts of TNF-α, which suggests that TNF-α production depends on the inflammation at the injection site.

Thus, subcutaneous vaccination with UV-F-V activates CD4$^+$ T cells in the regional lymph nodes as effectively as does vaccination with the UV-V vaccine; however, the cellular response generated by the doubly-inactivated vaccine is skewed towards a Th2-type response, whereas the UV-V vaccine induces a Th0-type response.

DISCUSSION

Various studies have demonstrated that vaccines based on whole, inactivated SARS-CoV potently elicit neutralizing antibodies in animal models (reviewed in [10]). We and others have prepared inactivated vaccines by using UV irradiation, formalin, or β-propiolactone treatment (14,23-25). Since whole inactivated vaccines must be completely safe before they can be applied to humans, we doubly inactivated SARS-CoV with UV irradiation and formalin to ensure the complete killing of the virus, and compared the immunogenicities of the UV-only (UV-V)- and UV+formalin (UV-F-V)-treated vaccines. We found that the formalin treatment did not impair the ability of the vaccine to elicit neutralizing antibodies, which play an important role in protecting the host from infection with SARS-CoV (10). While both humoral and cellular immune responses are known to contribute to protection against other animal coronavirus infections (26,27), Yang et al. found that the cellular immunity generated by their vaccine was not required for the inhibiyion of viral replication (9). Consequently, a whole SARS-CoV vaccine that is safe in humans due to inactivation by two methods and that potently generates neutralizing antibodies would be a significant resource in preventing further outbreaks of SARS.

Vaccines based on whole inactivated viruses have an advantage over other vaccine approaches in that the viral proteins, particularly conformation-dependent antigens such as the S protein, are abundantly expressed on the surface of virions. In contrast, in recombinant carrier viruses, such three-dimensional structures may be altered. Along these lines, See et al. found that a β-propiolactone-treated killed SARS-CoV vaccine generated more neutralizing antibodies and was more protective in mice than was a recombinant adenovirus vaccine expressing S and N (28). Their killed vaccine generated significantly higher SARS-CoV-specific IgG_{2a} antibodies than IgG_1 antibodies, and the SARS-CoV-specific IgG_1, but not the IgG_{2a}, response was significantly augmented by alum. These findings are consistent with our results ([14] and this study). Notably, we observed here that formalin treatment of UV-V suppressed the IgG_{2a} response. Since it is known that the antibody isotype profile reflects the T-cell immune response (29), this observation suggests that formalin treatment of UV-inactivated virions promotes Th2-type T-cell responses. In further support of this line of reasoning, the in vitro stimulated T cells from UV-F-V-vaccinated mice

produce higher levels of IL-4 than that produced by T cells from UV-V-vaccinated mice. As the present manuscript was under preparation, Moghaddam et al. reported that carbonyl groups on vaccine antigens created by formalin treatment profoundly affect immunogenicity and boost Th2 responses induced by the respiratory syncytial virus (RSV) vaccine in mice (30).

Recently, Spruth et al. examined the efficacy of a double-inactivated whole killed SARS-CoV vaccine (31), in which SARS-CoV was first inactivated with formalin and then by UV irradiation. This vaccine elicited high levels of neutralizing antibodies and protected the mice from intranasal challenge with SARS-CoV. ELISPOT analysis revealed that the vaccine stimulated both Th-1 (IFN-γ) and Th-2 (IL-4) type cellular immune responses (14). However, in that study, the immunogenic profile elicited by double-inactivated SARS-CoV vaccine was not compared to that generated by vaccine inactivated by just one approach. Another study by Zakhartchouk et al. has shown that whole inactivated SARS virus by beta-propiolactone induces a Th2-dominant T-cell response, and in combination with a DNA vaccine, Th1-type immune responses became dominant (32). In addition to the type of vaccine, other factors such as the vaccine formulation, the adjuvant, and the route of immunization are also known to affect the immune response that is generated. For instance, a whole inactivated influenza vaccine induced a Th1-dominant response, while a split virus vaccine elicited a Th2-biased response (33). Thus, the immunogenic profile in vivo generated by killed whole viruses can be altered by a range of different factors. Such variables need to be carefully examined during the development of inactivated vaccines.

In summary, this is the first study to compare the immune profiles generated by SARS-CoV virions that have been inactivated by UV irradiation only (UV-V) to those generated by virions inactivated by both UV and formalin (UV-F-V). Treating the virions with both UV and formalin is likely to greatly increase the safety of the vaccine. We found that booster immunization with UV-F-V+alum generated equivalent levels of neutralizing antibody to those elicited by immunization with the UV-V vaccine. Although no challenge experiments were carried out in this series, the present results suggest that UV-F-V is likely to be as protective as UV-V. Notably, we found that the additional formalin treatment skewed the cellular response towards the Th2 type, most likely as a result of the carbonyl groups generated by formalin, as was recently described by Moghaddam et al. (30) in the case of the RSV vaccine. Should cellular immunity be crucial for the efficacy of a vaccine (which may not be the case for SARS-CoV vaccines), it might be necessary to combine a whole inactivated virus with other Th1-inducing type vaccines.

ACKNOWLEDGMENTS

We greatly thank Mr. Masayuki Ishige, Ms. Sayuri Yamaguchi, Ms. Hiroko Kusachi and Ms. Reiko Iwaki for their excellent technical help.

This work was supported by grants that were funded in part by the Ministry of Health, Labour and Welfare and in part by the Ministry of Education, Culture, Sports, Science and Technology of Japan.

REFERENCES

1. Drosten, C., Gunther, S., Preiser, W., et al. (2003): Identification of a novel coronavirus in patients with severe acute respiratory syndrome. N. Engl. J. Med., 348, 1967-1976.
2. Ksiazek, T.G., Erdman, D., Goldsmith, C.S., et al. (2003): A novel coronavirus associated with severe acute respiratory syndrome. N. Engl. J. Med., 348, 1953-1966.
3. Holmes, K.V. and Enjuanes, L. (2003): Virology. The SARS coronavirus: a postgenomic era. Science, 300, 1377-1378.
4. Marra, M.A., Jones, S.J., Astell, C.R., et al. (2003): The genome sequence of the SARS-associated coronavirus. Science, 300, 1399-1404.
5. Li, W., Moore, M.J., Vasilieva, N., et al. (2003): Angiotensin-converting enzyme 2 is a functional receptor for the SARS coronavirus. Nature, 426, 450-454.
6. Wong, S.K., Li, W., Moore, M.J., et al. (2003): A 193-amino acid fragment of the SARS coronavirus S protein efficiently binds angiotensin-converting enzyme 2. J. Biol. Chem., 279, 3197-3201.
7. Li, G., Chen, X. and Xu, A. (2003): Profile of specific antibodies to the SARS-associated coronavirus. N. Engl. J. Med., 349, 508-509.
8. Clarke, T. (2003): SARS what have we learned? What about vaccine? Nature, 424, 126.
9. Yang, Z.Y., Kong, W.P., Huang, Y., et al. (2004): A DNA vaccine induces SARS coronavirus neutralization and protective immunity in mice. Nature, 428, 561-564.
10. Tsunetsugu-Yokota, Y., Ohnishi, K. and Takemori, T. (2006): Severe acute respiratory syndrome (SARS) coronavirus: application of monoclonal antibodies and development of an effective vaccine. Rev. Med. Virol., 16, 117-131.
11. Buchholz, U.J., Bukreyev, A., Yang, L., et al. (2004): Contributions of the structural proteins of severe acute respiratory syndrome coronavirus to protective immunity. Proc. Natl. Acad. Sci. USA, 101, 9804-9809.
12. Bukreyev, A., Lamirande, E.W., Buchholz, U.J., et al. (2004): Mucosal immunisation of African green monkeys (*Cercopithecus aethiops*) with an attenuated parainfluenza virus expressing the SARS coronavirus spike protein for the prevention of SARS. Lancet, 363, 2122-2127.
13. Ishii, K., Hasegawa, H., Nagata, N., et al. (2006): Inductionof protective immunity against severe acute respiratory syndrome coronavirus (SARS-CoV) infection using highly attenuated recombinant vaccinia virus DIs. Virology, 351, 368-380.
14. Takasuka, N., Fujii, H., Takahashi, Y., et al. (2004): A subcutaneously injected UV-inactivated SARS coronavirus vaccine elicits systemic humoral immunity in mice. Int. Immunol., 16, 1423-1430.
15. Ohnishi, K., Sakaguchi, M., Kaji, T., et al. (2005): Immunological detection of severe acute respiratory syndrome coronavirus by monoclonal antibodies. Jpn. J. Infect. Dis., 58, 88-94.
16. Liu, X., Shi, Y., Li, P., et al. (2004): Profile of antibodies to the nucleocapsid protein of the severe acute respiratory syndrome (SARS)-associated coronavirus in probable SARS patients. Clin. Diagn. Lab. Immunol., 11, 227-228.
17. Shi, Y., Yi, Y., Li, P., et al. (2003): Diagnosis of severe acute respiratory syndrome (SARS) by detection of SARS coronavirus nucleocapsid antibodies in an antigen-capturing enzyme-linked immunosorbent assay. J. Clin. Microbiol., 41, 5781-5782.
18. Faber, M., Lamirande, E.W., Roberts, A., et al. (2005): A single immunization with a rhabdovirus-based vector expressing severe acute respiratory syndrome coronavirus (SARS-CoV) S protein results in the production of high levels of SARS-CoV-neutralizing antibodies. J. Gen. Virol., 86, 1435-1440.
19. Gao, W., Tamin, A., Soloff, A., et al. (2003): Effects of a SARS-associated coronavirus vaccine in monkeys. Lancet, 362, 1895-1896.
20. Holmes, K.V. (2005): Structural biology. Adaptation of SARS coronavirus to humans. Science, 309, 1822-1823.
21. Slifka, M.K., Matloubian, M. and Ahmed, R. (1995): Bone marrow is a major site of long-term antibody production after acute viral infection. J. Virol., 69, 1895-1902.
22. Moran, T.M., Park, H., Fernandez-Sesma, A., et al. (1999): Th2 responses to inactivated influenza virus can Be converted to Th1 responses and facilitate recovery from heterosubtypic virus infection. J. Infect. Dis., 180, 579-585.
23. Qu, D., Zheng, B., Yao, X., et al. (2005): Intranasal immunization with inactivated SARS-CoV (SARS-associated coronavirus) induced local and serum antibodies in mice. Vaccine, 23, 924-931.
24. Xiong, S., Wang, Y.F., Zhang, M.Y., et al. (2004): Immunogenicity of SARS inactivated vaccine in BALB/c mice. Immunol. Lett., 95, 139-143.
25. Zhang, C.H., Lu, J.H., Wang, Y.F., et al. (2005): Immune responses in Balb/c mice induced by a candidate SARS-CoV inactivated vaccine prepared from F69 strain. Vaccine, 23, 3196-3201.
26. Jackwood, M.W. and Hilt, D.A. (1995): Production and immunogenicity of multiple antigenic peptide (MAP) constructs derived from the S1 glycoprotein of infectious bronchitis virus (IBV). Adv. Exp. Med. Biol., 380, 213-219.
27. Liu, J., Lim, S.L., Ruan, Y., et al. (2005): SARS transmission pattern in Singapore reassessed by viral sequence variation analysis. PLoS Med., 2, e43.

28. See, R.H., Zakhartchouk, A.N., Petric, M., et al. (2006): Comparative evaluation of two severe acute respiratory syndrome (SARS) vaccine candidates in mice challenged with SARS coronavirus. J. Gen. Virol., 87, 641-650.
29. Stevens, T.L., Bossie, A., Sanders, V.M., et al. (1988): Regulation of antibody isotype secretion by subsets of antigen-specific helper T cells. Nature, 334, 255-258.
30. Moghaddam, A., Olszewska, W., Wang, B., et al. (2006): A potential molecular mechanism for hypersensitivity caused by formalin-inactivated vaccines. Nat. Med., 12, 905-907.
31. Spruth, M., Kistner, O., Savidis-Dacho, H., et al. (2006): A double-inactivated whole virus candidate SARS coronavirus vaccine stimulates neutralising and protective antibody responses. Vaccine, 24, 652-661.
32 Zakhartchouk, A.N., Liu, Q., Petric, M. et al. (2005): Augmentation of immune responses to SARS coronavirus by a combination of DNA and whole killed virus vaccines. Vaccine, 23, 4385-4391.
33 Hovden, A.O., Cox, R.J. and Haaheim, L.R. (2005): Whole influenza virus vaccine is more immunogenic than split influenza virus vaccine and induces primarily an IgG2a response in BALB/c mice. Scand. J. Immunol., 62, 36-44.

JVI Accepts, published online ahead of print on 14 March 2007
J. Virol. doi:10.1128/JVI.02811-06

Enhanced Replication of Human T-cell Leukemia Virus Type 1 in T Cells from Transgenic Rats Expressing Human CRM1 That Is Regulated in a Natural Manner

Ryo Takayanagi[1], Takashi Ohashi[1], Eizaburo Yamashita[2], Yohei Kurosaki [1], Kumiko Tanaka[1], Yoshiyuki Hakata[1,6], Yasumasa Komoda[3], Satoru Ikeda[3], Yasuko Tsunetsugu-Yokota[4], Yuetsu Tanaka[5], Hisatoshi Shida[1]*

[1]Institute for Genetic Medicine, Hokkaido University, Kita-ku, Sapporo 060-0815, Japan

[2] Department of Orthopaedic Surgery, Graduate School of Medicine, Kyoto University, Kyoto, Japan

[3]Central Pharmaceutical Research Institute, Japan Tobacco Inc., Takatsuki, Osaka 569-1125, Japan

[4] Department of Immunology, National Institute of Infectious Diseases, Shinjuku-ku, Tokyo 162-8640, Japan

[5] Department of Immunology, Graduate School and Faculty of Medicine, University of the Ryukyus, Nishihara, Okinawa 903-0215, Japan

[6] Present sddress: Department of Microbiology, NYU school of Medicine, 522 First Avenue, New York, New York 10016, USA

*Corresponding author: Hisatoshi Shida, Institute for Genetic Medicine, Hokkaido University, Kita-15, Nishi-7, Kita-ku, Sapporo 060-0815, Japan.
E-mail:hshida@igm.hokudai.ac.jp. Phone/Fax number:81-11-706-7543

Running title: HTLV-1 replication in hCRM1 Tg rat

Word counts Abstract: 221
Text: 6015

Abstract

Human T-cell leukemia virus type 1 (HTLV-1) is the etiologic agent of adult T cell leukemia (ATL). To develop a better animal model for the investigation of HTLV-1 infection, we established a transgenic (Tg) rat carrying the human CRM1 (hCRM1) gene that encodes a viral RNA transporter, which is a species-specific restriction factor. At first we found that CRM1 expression is elaborately regulated through protein kinase C involving pathway during lymphocyte activation initially by post-transcriptional and subsequently by transcriptional manners. This fact led us to use an hCRM1 containing BAC clone, which would harbor the entire regulatory and coding regions of the CRM1 gene. The Tg rats expressed hCRM1 protein in a manner similar to the intrinsic rat CRM1 in various organs. HTLV-1-infected T cell lines derived from these Tg rats produced 100 to 10,000 fold more HTLV-1 than did T cells from wild type rats, and the absolute levels of HTLV-1 were similar to those produced by human T cells. We also observed enhancement of the dissemination of HTLV-1 to thymus in the Tg rats after intraperitoneal inoculation, although the proviral loads were low both in wild type and the Tg rats. These results support the essential role of hCRM1 in proper HTLV-1 replication and suggest the importance of this Tg rat as an animal model for HTLV-1.

45 **INTRODUCTION**

46

47 Human T-cell leukemia virus type I (HTLV-1) is etiologically associated with human adult
48 T-cell leukemia (ATL), a chronic progressive neurological disorder termed HTLV-1
49 associated myelopathy/tropical spastic paraparesis (HAM/TSP) (17, 27, 54, 55), and several
50 other human diseases (23, 40, 42, 48). Examination of the viral nucleotide sequences among
51 different disease groups has not revealed any specific determinants that distinguish a
52 particular HTLV-1 associated disease (11, 35, 67). Thus, a primary determinant of HTLV-1
53 associated disease may be host-related.

54 In order to investigate HTLV-1 infection and its related disease development in detail,
55 suitable animal models are required. HTLV-1 can immortalize simian, feline, rat, and rabbit
56 lymphocytes *in vitro* (2, 29, 46). HTLV-1 can also infect experimental animals, such as
57 rabbits, monkeys, and rats (2, 45, 53, 62). Using these susceptible animals, several models
58 have been developed to study HTLV-1 associated diseases. The HAM/TSP-like disease
59 model in WKA strain rats has been well established and used to dissect the pathogenic
60 mechanisms of the disease (31, 39). In contrast, only a few ATL model systems have been
61 established using rabbits and rats, but their utility is limited. For instance, the rabbit ATL
62 model shows reproducible development of an ATL-like disease in adult animals (58), but few
63 immunological studies can be performed in this animal, primarily because of the difficulty in
64 obtaining inbred strains of rabbits. In the rat models, the development of ATL-like disease
65 was observed only in newborn animals with a very short period of disease onset (64), making
66 it difficult to perform oncological and immunological studies at the same time. Kannagi and
67 Ohashi have established a rat model of ATL-like disease in which they were able to examine
68 the growth and spread of HTLV-1-infected cells, as well as assess the effects of T cells on the
69 development of the disease in T cell-deficient nude rats (51). This model system has been
70 used to assess DNA or peptide-based vaccine development (25, 52) and to study the effects of
71 Tax-directed siRNA on HTLV-1 induced tumors (50). However, since the growth of HTLV-1
72 tumors could be monitored in only immune-deficient nude rats in this model system, better
73 animal models are still necessary.

HTLV-1 replicates poorly in rats, which may be one of the reasons why previously established models could not completely reproduce the features of HTLV-1 related diseases. We have previously examined the differences in the pattern of viral gene expression between human and rat T cells infected with HTLV-1. In rat cells, the levels of viral mRNAs encoding the Gag and Env proteins were much lower than those encoding the Tax and Rex proteins (36). Rex plays an important role in escorting unspliced and incompletely spliced viral mRNAs to the cytoplasm, resulting in enhanced synthesis of viral structural proteins (5, 34, 69). Human CRM1 (hCRM1) is a critical factor for Rex-dependent viral mRNA export to the cytoplasm and rat CRM1 (rCRM1) cannot substitute for this function (19, 22, 69). Thus, it is reasonable to assume that transgenic (Tg) rats carrying the hCRM1 gene should provide a better environment for HTLV-1 replication and that such animals would provide a better animal model of HTLV-1 infection.

CRM1 is involved in numerous cellular activities, suggesting its essential function in viability, which is supported by the high conservation of CRM1 genes from yeast to humans (37) and by the demonstration that both yeast and mammalian cells defective for CRM1 are inviable (1, 15). In contrast, overexpression of CRM1 has been reported to inhibit early embryogenesis in Xenopus (8). Therefore, proper expression of hCRM1 in rats will be essential to produce Tg rats. However, the regulation of CRM1 expression and synthesis has not yet been investigated in detail. Some immortalized cell lines have been reported to maintain CRM1 protein at constant levels throughout the cell cycle, which is compatible with an essential function (37), but other reports have indicated variations in the level of expression of CRM1 among different tissues (28, 37), implying that the expression is regulated. Therefore, we first investigated the expression profile of the CRM1 gene, especially during lymphocyte activation, to determine means for the proper expression of hCRM1 as a transgene. Our results indicate that expression of the CRM1 gene is elaborately regulated during activation of lymphocytes, including $CD4^+$ T cells, the major targets of HTLV-1. These data suggested that it would be necessary to use a construct harboring the entire regulatory and coding regions of CRM1 for Tg rat construction.

Using an artificial bacterial chromosome (BAC) clone containing the entire CRM1 gene, we have established hCRM1 Tg rats and examined the proliferation of HTLV-1 in vitro and in vivo. Our results demonstrate that T cell lines isolated from hCRM1 Tg rats produced 100 to 10,000 times more HTLV-1 Gag antigen compared to T cells from wild type control rats and that Tg rats displayed a more extensive invasion of HTLV-1 into the thymus when infected intraperitoneally. These results indicate the essential role of hCRM1 in proper HTLV-1 replication and suggest the importance of this Tg rat model as a basis for the development of better HTLV-1 animal models.

MATERIALS AND METHODS

Cells. Peripheral blood mononuclear cells (PBMCs) were isolated from healthy donors using Ficoll-Hypaque (Pharmacia) or Ficoll Paque Plus (Amersham Biotechnology) density centrifugation. $CD4^+$ T lymphocytes were purified by negative selection using an immunomagnetic cell sorting apparatus, the MidiMACS cell separator (Miltenyi Biotec), using a cocktail of MACS MicroBeads coupled to hapten-conjugated MAbs specific for CD8, CD11b, CD16, CD19, CD36, and CD56. The purity of $CD4^+$ T cells was evaluated by flow cytometry (FACSCalibur: BECTON DICKINSON) to be approximately 95% pure.

For activation, cells were cultured with various combinations of 50 nM phorbol 12-myristate 13-acetate (PMA), 100 nM ionomycin, and 10 ng/ml IL-2.

The HTLV-1 producing rat and human T cell lines, FPM1 and MT-2, have been described previously (36, 44). HTLV-1-immortalized cell lines from wild type (Wt) or Tg rats were established by cocultivating thymocytes or splenocytes with MT-2, which had been treated with mitomycin C (50 μg/ml) for 30 min at 37°C. These cells were maintained in the medium supplemented with 10 U/ml of interleukin (IL)-2 (PEPROTECH EC) at the beginning of co-culture. Some cell lines were eventually freed from exogenous IL-2.

Western blotting. Cells were lysed in ice-cold extraction buffer (10 mM Tris-HCl [pH 7.4], 1 mM $MgCl_2$, 0.5% NP-40) containing protease inhibitor cocktail (Complete mini; Roche Diagnostics). The protein concentration of each sample was determined using a protein assay

kit (QB PERBIO; Pierce). The cell lysates were sonicated, or in some cases treated with DNase 1 solution (Takara), then dissolved in sample buffer. The same amounts (approximately 20 μg) of cell lysates were subjected to SDS-PAGE. Following electrophoresis. Proteins were transferred to a nitrocellulose membrane and probed with anti-human or rat CRM1(34), anti-β-actin (AC40; Sigma), or anti-Rex (34) antibodies followed by secondary antibodies conjugated to alkaline phosphatase or horseradish peroxidase. Proteins were visualized by staining with BCIP/NBT, or ECL+ (Amersham Pharmacia Biotech) followed by the LAS-100 plus system (Fuji film) and evaluated by Image Gauge Version 3.4 software (Fuji film).

hCRM1 mRNA quantitative RT-PCR. Total RNA was extracted using the RNeasy Mini Kit (Qiagen) and treated with RNase-Free DNase I (Qiagen) to minimize contamination of chromosomal DNA. The RNA concentration was measured by absorbance at 260 nm, and purity was ascertained by the OD 260/280 ratio and gel electrophoresis.

To quantify CRM1 mRNA, RNA samples (5 μg) were subjected to quantitative RT-PCR with the Platinum Quantitative RT-PCR Thermoscript One Step System (Invitrogen) using the forward primer 5'- GCT GAA AAC TCA ACC GAG ATG G -3' and the reverse primer 5'- CTG TTG CTC TTG CTG ATG CTG TA -3', and a probe (FAM-) AAA ATG CCG CAG GCA TTT CGT TCA G (-TAMRA). RT-PCR was performed by incubating for 2 min at 50 °C, 30 min at 60 °C, 10 min at 95 °C, and then 50 cycles of 20 s at 95 °C and 1 min at 62 °C in an Applied Biosystems Prism 7700 Sequence Detector Thermocycler (Applied Biosystems) with Sequence Detector software (Applied Biosystems). To make standard curves, the region from -943 to +38 bp of the CRM1 cDNA was amplified by PCR using Human Lung Marathon Ready cDNA (Clontech) with adaptor primer-1 and 5'-GCTGCATGGTCTGCTAACATT-3' and by nested PCR with adaptor primer-2 and 5'-CTGCATGGTCTGCTAACATTG-3'. The PCR product was cloned into the vector pCR 2.1 (Invitrogen) and a 981-base single stranded RNA was synthesized *in vitro* with MegaScript T7 (Ambion).

Establishment of human CRM1 transgenic rats. pBeloBAC hCRM1, which harbors the entire human CRM1 genomic sequence including approximately 50 kb of 5' upstream

sequence and 10 kb of 3' downstream sequence, was microinjected into 450 fertilized one-cell eggs prepared from Fischer 344/Du Crj (F344) female rats by the YS institute. Integration of the transgene was confirmed by PCR using genomic DNA, which was extracted by the PUREGENE™ tissue kit (Gentra) from the rat tail, as a template with the hCRM1 specific primer pairs: 5'-TTATGTGGCTGCAGTGTGGA-3' and 5'-ACATACCAGGGTTCTCTGGA-3', and 5'-GTCACCTGATGTCGGGAGTT-3' and 5'-GGATTACAGGTGTGAGCCA-3. All animal experiments were conducted according to the Guide for the Care and Use of Laboratory Animals, Institute for Genetic Medicine, Hokkaido University.

Detection of genomic copies of hCRM1 and G3PDH. Genomic DNA was subjected to PCR with the following primer pairs: hCRM1, forward primer (5'-TGA GGT CAG GAG TTC AGG AT-3') and reverse primer (5'-CTC TGC CTC CTG GGT TCA A-3'); G3PDH, forward primer (5'-AGA GCT GAA CGG GAA G-3') and reverse primer (5'-GGA AGA ATG GGA GTT GC-3'). The PCR conditions were: 5min at 94 °C, 10 cycles of 30 s at 94 °C, 60 s at 69 °C, with a decrease of 0.5 °C/cycle, and 30 s at 72 °C, followed by 8 cycles of 30 s at 94 °C, 60 s at 65 °C, and 30 s at 72 °C and a final extension for 10 min at 72 °C.

Quantification of HTLV-1 proviral load by LightCycler-based real-time PCR. The HTLV-1 proviral loads of HTLV-1-infected cells were quantified by real-time PCR on a LightCycler PCR Instrument (Roche Diagnostics). Briefly, 20 μl of a PCR mixture in a capillary tube containing each HTLV-1 pX-specific inner primer pair at 0.4 μM, 1x LightCycler-FastStart SYBR Green PCR Master Mix, and 30 ng of genomic DNA was subjected to 40 cycles of denaturation (95 °C 15 s), annealing (69 °C, 10 s), and extension (72 °C, 10 s) following an initial Taq polymerase activation step (95 °C, 15 min). The copy numbers of HTLV-1 provirus in the samples were estimated from a standard regression curve using the LightCycler Software version 3 (Roche Diagnostics). The standard curve for HTLV-1 provirus was obtained by PCR data using $1x10^2$ to $1x10^8$ copies of pCR-pX1-4 plasmids, which were constructed by inserting a PCR fragment amplified with pX1 (5'-CCC ACT TCC CAG GGT TTG GAC AGA GTC TTC-3') and pX4 (5'-GGG GAA GGA GGG GAG TCG AGG GAT AAG GAA-3') from the genomic DNA of MT-2 cells into pCR2.1.

189 The copy numbers of HTLV-1 provirus were normalized by dividing with those of the
190 G3PDH gene in the same samples.
191 **Detection of HTLV-1 p19.** Each cell line (10^5/well) was cultured in 24-well flat-bottom
192 plates for 4 days. The amount of HTLV-1 p19 protein in the culture supernatant or in rat
193 plasma was quantified using HTLV-1/2 p19 antigen ELISA (ZeptoMetrix).
194 **Detection of intracellular Tax and Gag protein.** Cells (10^6) were fixed with 1%
195 paraformaldehyde in phosphate-buffered saline (PBS) containing 20 μg/ml of lysolecithin
196 (Sigma) for 2 min at room temperature, centrifuged, and resuspended in cold methanol. The
197 cells were then sorted at 4 °C for 15 min, centrifuged, and incubated in 0.1% NP40 in PBS at
198 4 °C for 5 min. After centrifugation, the cells were stained with mouse anti-Tax MAb LT-4
199 (63) or the mouse anti-Gag MAb GIN-7 (38) followed by FITC-conjugated goat anti-mouse
200 IgG plus M antibody (Immunotech). Finally, the cells were washed and fixed with 1%
201 formalin in PBS prior to analysis by cell sorting.
202 **Inoculation of HTLV-1 into rats.** Various numbers of mitomycin C-treated or untreated
203 MT-2 cells were intraperitoneally administered to 3 to 6 week old Wt or hCRM1-Tg rats.
204 Peripheral blood samples were collected from the rats every 2 or 4 weeks after inoculation
205 and the presence of HTLV-1 provirus in peripheral blood cells and levels of p19 in plasma
206 were determined. In some experiments, rats were euthanized 1 week after inoculation and
207 samples were collected to assess plasma p19 concentrations, proviral loads, and the presence
208 of HTLV-1 provirus.
209 **Detection of provirus in HTLV-1-infected rats.** To determine the positive rate of HTLV-1
210 provirus in various organs, 200 μg of genomic DNA was subjected to PCR for the
211 amplification of the px region of HTLV-1 as described previously (51). The first-step PCR
212 was performed with the primer pair of pX1 and pX4, followed by the second-step PCR with
213 the primer pair of pX2 (5'-CGGATACCCAGTCTACGTGTTTGGAGACTGT-3') and pX3
214 (5'-GAGCCGATAACGCGTCCATCGATGGGGTCC-3'). The PCR conditions were:
215 activation of Taq polymerase (94 °C, 3 min); 35 cycles of denaturation (94 °C, 30 sec),
216 annealing (60 °C, 30 sec), and extension (72 °C, 30 sec), and a final elongation of the product

(72 °C, 3 min). For a nested PCR, an aliquot of the first PCR product was subjected to another 35 PCR cycles with the second set of primers.

RESULTS

Regulated expression of CRM1 in lymphocytes. We first examined the level of expression of CRM1 mRNA in human tissues by PCR using cDNA derived from the tissues. Expression of CRM1 mRNA was variable in different tissues. Notably, CRM1 mRNA was expressed at very low levels in PBMCs (data not shown). This result was unexpected because PBMCs include $CD4^+$ T cells, which are the targets of HIV and HTLV-1 (14). Lymphocytes in the PBMC population are mainly in a resting state, leading us to hypothesize that the production of CRM1 is stimulated during lymphocyte activation. Consequently, activated hematopoietic cells should contain CRM1 protein at levels similar to those observed in lymphocyte derived cell lines. We prepared $CD4^+$ T helper cells, macrophages, and DCs from PBMCs, cultured them in the presence of appropriate cytokines, and compared the amount of CRM1 present in these cells with amounts found in Jurkat cells, a transformed cell line that constitutively expresses CRM1. Western blotting indicated that all activated lymphocyte subsets and monocyte-lineage cells expressed CRM1 at levels similar to those in Jurkat cells (data not shown). These results indicate that lymphocyte activation induces high levels of CRM1 expression.

To demonstrate that CRM1 is induced during lymphocyte activation, we stimulated freshly isolated PBMCs with calcium ionophore, PMA, and IL-2, and examined CRM1 levels at several times by Western blotting (Figure 1A). The level of CRM1 in resting PBMCs was very low. The level of CRM1 clearly increased 4 h after stimulation, and then gradually increased further, up to 72 h, although some differences were observed between donors 1 and 2. Little change in the level of CRM1 was observed in the absence of stimulation. Actin was used as a loading control, as its level remained relatively constant. These results indicate that the CRM1 gene belongs to the class of early response genes that are induced during lymphocyte activation.

We next measured the levels of CRM1 mRNA by quantitative RT-PCR to determine how the expression of CRM1 is stimulated in PBMCs (Figure 1B). The amount of CRM1 transcript did increase, but the expression profile varied among individuals. For example, the level of CRM1 mRNA observed in donor 3 was relatively constant up to 24 h after stimulation and then started to increase, while the level of CRM1 mRNA in donor 1 gradually increased over the course of activation. Nevertheless, we consistently found in 4 experiments that the increase in CRM1 mRNA occurred after the increase in CRM1 protein. Specifically, up to 4 h after stimulation, marked increases in the level of CRM1 protein were detected, in contrast to nearly constant levels of CRM1 mRNA. Therefore, these results suggest that during lymphocyte activation CRM1 production is initially stimulated post-transcriptionally and then further enhanced by upregulating transcription.

In order to identify the signaling pathway responsible for the induction of CRM1 transcription, we activated PBMCs in the presence of various combinations of IL-2, calcium ionophore, and PMA. As shown in Figure 1C, IL-2 and PMA fully induced CRM1 whereas IL-2 and calcium ionophore did not. Next, we examined whether PMA alone is sufficient to induce CRM1. PMA alone enhanced CRM1 production as efficiently as IL-2 plus PMA. Since PMA is an activator of protein kinase C (PKC) (49), these data suggest that induction of CRM1 is PKC dependent.

To confirm the above results, we examined the effect of various inhibitors including staurosporine (a PKC inhibitor) (60) and cyclosporin (a Ca^{++} cascade inhibitor) (66). As shown in Figure 1D, staurosporine, but not cyclosporin, inhibited the induction of CRM1, consistent with the results shown in Figure 1C. We further examined the effects of PDTC (an NFkB inhibitor) (43) and PD98059 (a MAPKK inhibitor) (3) and found that PDTC inhibited CRM1 induction at the highest dose, but PD98059 had only a minor effect.

Regulated expression of CRM1 in $CD4^+$ T lymphocytes. To examine CRM1 regulation in $CD4^+$ T lymphocytes, resting $CD4^+$ T lymphocytes were purified by negative selection and activated by treatment with a combination of IL-2, ionophore, and PMA. CRM1 levels were estimated by Western blotting (Figure. 2A). CRM1 expression was induced by the same stimuli as in PBMCs, although the kinetics of induction was somewhat different among

donors. In contrast to CRM1, the level of actin was constant during T cell activation. Staurosporine inhibited the enhanced production of CRM1 (data not shown), indicating the involvement of PKC in the induction of CRM1 in $CD4^+$ T cells.

To examine the mechanism underlying the stimulation of CRM1 in $CD4^+$ T cells, we measured the amount of CRM1 mRNA by quantitative RT-PCR (Figure 2B). Similar to PBMCs, the amount of CRM1 mRNA also increased during $CD4^+$ T cell activation. Although the levels of CRM1 mRNA during T cell activation varied to some extent among donors, similar profiles of induction were observed; after a lag of approximately 4 h, the level of CRM1 mRNA started to increase and continued to do so for up to 24 h after stimulation. These results suggest that the increase in CRM1 mRNA is delayed compared to the increase in CRM1 protein, as seen in PBMCs. The level of CRM1 mRNA was constant at times greater than 24 h post-stimulation, but purified $CD4^+$ T cells appeared unhealthy 2 and 3 days after stimulation in these cultures, as judged by microscopic observation. Therefore, further examination is required to definitively determine the levels of CRM1 protein and mRNA in $CD4^+$ T cells at later times after stimulation.

Expression of hCRM1 in the Tg rat. The above results indicate that regulation of CRM1 expression during the activation of lymphocytes is complex. Considering the lack of characterization of CRM1 regulatory elements, we used a BAC clone, which is likely to harbor the entire regulatory and coding regions of the CRM1 gene, to establish an hCRM1-Tg rat. One rat strain carrying the hCRM1 transgene was obtained from microinjection of the hCRM1 containing BAC clone into 450 fertilized one-cell eggs from F344 female rats. We assessed the expression of hCRM1 protein in each tissue by immunoblotting using hCRM1 specific antibody (22). As shown in Figure 3A, hCRM1 expression was detected in all organs tested. The expression level of this protein was especially high in ovary and thymus compared to other organs. In addition, expression levels of hCRM1 in the organs were similar to those of endogenous rCRM1 (Figure 3B). hCRM1 expression was not detected in any organs prepared from wild type rats (data not shown). These data indicate that the Tg rats express hCRM1 in a physiologically relevant manner.

303 **Enhanced production of p19 Gag in Tg-derived cell lines.** To assess the replication of
304 HTLV-1 in T cells of hCRM1 Tg rats, we established several T cell lines from both Wt and
305 Tg rats by infecting with HTLV-1. Thymocytes and splenocytes isolated from Wt or hCRM1-
306 Tg rats were co-cultured with the HTLV-1-infected human T cell line MT2, which had been
307 treated with mitomycin C and then maintained in culture medium containing 10 U/ml of IL-2.
308 After 2 months of cultivation, we obtained 6 lines from Wt rats and 11 from Tg rats (Table 1).
309 As shown in Figure 4, all of the Tg-derived cell lines were confirmed to have the hCRM1
310 gene (Figure 4A) and express hCRM1 (Figure 4B), whereas none of Wt-derived lines
311 contained the gene or the protein. The expression level of hCRM1 was different among the
312 cell lines.
313 We next examined the expression of cell surface markers, including CD3, CD4, CD5, CD8,
314 CD25, MHC-I, and MHC-II, in these cell lines (Table 1). All the cell lines expressed rat
315 CD25 and MHC-I, indicating that they were derived from rat cells, not from the human MT2
316 cells. Most of the cell lines also expressed rat CD5 and MHC-II, with the exception of 2 Wt
317 and 3 Tg-derived lines. Expression of rat CD3 was confirmed in 6 of 9 Tg lines, whereas only
318 2 of 6 lines were positive in the Wt lines. Rat CD4 expression was detected in 1 Wt and 6 Tg
319 cell lines. Rat CD8 was detected in 1 Wt and 1 Tg-derived line. As judged by the expression
320 of CD3, we established a total of 8 T cell lines, 2 from Wt and 6 from Tg rats.
321 We next examined the production of the p19 Gag protein in the cell lines to assess the effect
322 of hCRM1 on HTLV-1 replication. Our results demonstrated that the Tg-derived cell lines
323 produced much greater levels of p19 in the culture supernatant, compared to the Wt-derived
324 cells (Figure 4C). After 2 and 4 days in culture, the mean p19 production by 9 Tg-derived cell
325 lines was 1000 ± 10 and 10000 ± 100 times higher, respectively, than the mean production of
326 the 6 Wt-derived lines (Figure 4D). The amounts (1-60 ng/ml) of p19 released from the Tg-
327 derived cell lines are equivalent to human HTLV-1 producing T cell lines, such as MT2 and
328 MT4 (data not shown). These results clearly demonstrate the enhanced production of the
329 HTLV-1 Gag protein in the cells expressing hCRM1.
330 To further examine the increased p19 production in each cell line expressing hCRM1, we
331 conducted a FACS analysis to detect the intracellular Gag protein. As shown in Figure 4E, we

were able to detect p19 and the precursor p55 Gag protein in all cell lines derived from Tg rats. In contrast, no Wt-derived cell lines produced detectable amounts of Gag. These results further support the role of hCRM1 in the enhancement of HTLV-1 Gag production.

We also assessed the proliferation of each cell line to exclude the possibility that the enhanced production was not due to increased production by individual cells, but was the result of increases in the number of cells in the Tg-derived lines. As shown in Figure 4F, we confirmed that there was no difference in the proliferation rate between Wt- and Tg-derived cell lines after 2 or 4 days in culture. In addition, there was no correlation between the rate of cell growth and the amount of p19 in the culture in any cell line.

The state of HTLV-1 infection is not correlated with levels of p19 production. We also assessed the proviral load of each cell line to rule out the possibility that enhanced production of Gag was due to increased provirus numbers in Tg cell lines. Real-time PCR analysis using a pair of primers for the Tax gene was performed to quantify the number of integrated provirus. As a relative standard, we used genomic DNA from FPM1 cells, which contain 3 copies of HTLV-1 provirus per cell (36). As shown in Figure 5A, all 5 Wt cell lines contained more than 2 copies of the provirus, whereas most of the Tg lines appeared to have only one provirus per cell, with the exception of FCCT13-1 cells which possessed 4 copies. Thus, there was no correlation between the provirus number and p19 production, indicating that differences in the amount of provirus were not responsible for the enhanced Gag production in Tg derived cells.

Altered expression of Tax and Rex could also be associated with enhanced expression of Gag in Tg-derived cells. Thus, we investigated the expression of Tax in the cell lines. As shown in Figure 5B, FACS analysis revealed that all of the cell lines tested expressed detectable levels of Tax proteins. Although we observed variations in the levels of Tax expression among the cell lines, there was no significant difference in the expression between Wt- and Tg-derived lines.

We next examined Rex expression by immunoblotting. As shown in Figure 5C, the Rex protein was expressed in all cell lines tested. Again, there was no statistical difference in the protein expression between Wt and Tg cells. Two Tg cell lines, FCMS1 and FCMS18,

expressed p21 protein as well as the p27 Rex. This expression was not associated with elevated expression of Gag, since the amounts of p19 Gag produced by these two cell lines were similar to the other Tg-derived cell lines (Figure 4C, D). These results indicate that the number of integrated provirus and the expression levels of Tax and Rex are not correlated with the enhanced expression of Gag observed in cell lines derived from hCRM1-Tg rats.

Enhanced Dissemination of HTLV-1 in hCRM1 Tg rats. We next examined the proliferation of HTLV-1 in Tg rats by inoculating animals with the HTLV-1 producing human T cell line MT2 as a virus source. Analysis of plasma p19 concentration in the infected rats over time did not show significant differences between Tg and Wt rats, although the p19 concentration in Tg rats tended to be higher during the first 6 weeks after infection (Figure 6A). Figure 6B shows the mean plasma p19 concentration in rats after 1 week of infection and again demonstrates higher, but not significantly different, levels of the viral protein in Tg-derived samples. To evaluate dissemination of the virus in vivo, we determined the presence of HTLV-1 provirus DNA in various organs 1 week after intraperitoneal infection by nested PCR that specifically amplifies a part of the px region. We calculated the percentage of rats that sustained the px gene in 5 independent experiments, and found that the rate with which the virus disseminated to the thymus in Tg rats was significantly higher than that in Wt rats (Figure 6C). However, we have not detected notable differences between the two groups in HTLV-1 proviral load detected in various organs including peripheral blood cells and thymus (Figure 6D, E, and data not shown). These results indicate the limited effects of hCRM1 in the proliferation of HTLV-1 in vivo, which are in dramatic contrast to the significant enhancement of HTLV-1 production in Tg derived cells in vitro.

DISCUSSION

Unlike hCRM1, rCRM1 does not support Rex function due to its inability to induce Rex-Rex dimerization, which is required for RNA export from the nucleus to the cytoplasm (22). This may be one reason why HTLV-1 replicates poorly in rats compared to humans. This

389 observation suggests the hCRM1-Tg rats would be novel animal models, since they would
390 support better replication of HTLV-1.
391 The essential role of CRM1 in cell viability suggested that proper expression of the
392 transgene would be a key for successful construction of Tg rats. Therefore, we examined the
393 expression pattern of CRM1 and found that CRM1 is expressed in a manner similar to the
394 early response genes induced during the activation of lymphocytes, including $CD4^+$ T cells.
395 Our results suggest that expression of CRM1 is stimulated in two steps: in the first phase,
396 lasting approximately 4 h, induction is regulated primarily in a post-transcriptional manner,
397 and in the second phase, transcriptional augmentation takes place. Alternatively, CRM1
398 protein in PBMCs may be rapidly turned over and is then protected from degradation upon
399 stimulation, giving rise to the early increase in protein levels. The profile of CRM1
400 expression further suggests that the initial induction occurs in the G_1 phase of the cell cycle,
401 which is also supported by the observation that mimosine, which blocks the cell cycle in late
402 G_1 (65), does not prevent the induction (data not shown).
403 The elaborate regulation of CRM1 expression led us to use a BAC clone harboring the entire
404 hCRM1 gene for Tg rat construction. An initial unsuccessful trial using the mouse H2
405 promoter to express hCRM1 cDNA supports the necessity of using the hCRM1 BAC. Our
406 results indicate that the hCRM1 BAC Tg rats express hCRM1 in various organs including
407 thymus and spleen, in a manner similar to endogenous rCRM1 in rats. Moreover, the
408 distribution of hCRM1 in the Tg rats is similar to that observed in humans (28, 37). Therefore,
409 use of the hCRM1 BAC construct may have resulted in physiological expression of the
410 protein in Tg rats. We also demonstrated hCRM1 expression in all Tg derived cell lines,
411 which will be useful for the functional analysis of hCRM1 in HTLV-1-infected cells.
412 We have previously reported that expression of hCRM1 induced an increase in HTLV-1
413 Gag production in both rat epithelial and T cells (21, 69). Our present study also showed that
414 T cell lines established from hCRM1-Tg rats produced significantly greater amounts of p19
415 than cell lines established from Wt rats, further indicating the positive effect of hCRM1 on
416 viral protein synthesis. This effect was not due to the effects of Tax or Rex proteins, which
417 enhance the transcription of total viral mRNAs and the nuclear export of unspliced and